1RS.1BL molecular resolution provides novel contributions to wheat improvement

Zhengang Ru[1,†], Angela Juhasz[2,†], Danping Li[3,†], Pingchuan Deng[4,†], Jing Zhao[3,†], Lifeng Gao[3,†], Kai Wang[5,†], Gabriel Keeble-Gagnere[6], Zujun Yang[7], Guangrong Li[7], Daowen Wang[8], Utpal Bose[9], Michelle Colgrave[2,9], Chuizheng Kong[3], Guangyao Zhao[3], Xueyong Zhang[3], Xu Liu[3], Guoqing Cui[3], Yuquan Wang[1], Zhipeng Niu[1], Liang Wu[4], Dangqun Cui[8]*, Jizeng Jia[8,3]*, Rudi Appels[10,6]* and Xiuying Kong[3]*

[1] School of Life Science and Technology, Henan Institute of Science and Technology, Xinxiang, China

[2] School of Science, Edith Cowan University, Joondalup, Australia

[3] The National Key Facility for Crop Gene Resources and Genetic Improvement, Institute of Crop Sciences, Chinese Academy of Agricultural Sciences, Beijing, China

[4] State Key Laboratory of Rice Biology, College of Agriculture and Biotechnology, Zhejiang University, Hangzhou, China

[5] Novogene Bioinformatics Institute, Beijing, China

[6] Agriculture Victoria Research, AgriBio, Centre for AgriBioscience, Bundoora, VIC, Australia

[7] Center for Informational Biology, School of Life Science and Technology, University of Electronic Science and Technology of China, Chengdu, China

[8]College of Agronomy, Collaborative Innovation Center of Henan Grain Crops, Henan Agricultural University, Longzi Lake Campus, Zhengzhou, China

[9] CSIRO Agriculture and Food, 306 Carmody Rd, St Lucia, Australia

[10] University of Melbourne, Parkville, Australia

[†]These authors contributed equally to this article.

*Correspondence: (e-mails dangquncui@163.com; jiajizeng@caas.cn; rudi.appels@unimelb.edu.au; kongxiuying@caas.cn).

Keywords: wheat, 1RS.1BL translocation, high-resolution structure and gene complement, gene families.

SUMMARY

Wheat-rye 1RS.1BL translocation has a significant impact on wheat yield and hence food production globally. However, the genomic basis of its contributions to wheat improvement is undetermined. Here, we generated a high-quality assembly of 1RS.1BL translocation comprising 748,715,293 bp with 4,996 predicted protein-coding genes. We found the size of 1RS is larger than 1BS with the active centromere domains shifted to the 1RS side instead of the 1BL side in Aikang58 (AK58). The gene alignment showed excellent synteny with 1BS from wheat and genes from 1RS were expressed well in wheat especially for 1RS where expression was higher than that of 1BS for the grain-20DPA stage associated with greater grain weight and negative flour quality attributes. A formin-like-domain protein FH14 (*TraesAK58CH1B01G010700*) was important in regulating cell division. Two PPR genes were most likely the genes for the multi fertility restoration locus Rf^{multi}. Our data not only provide the high-resolution structure and gene complement for the 1RS.1BL translocation, but also defined targets for enhancing grain yield, biotic and abiotic stress, and fertility restoration in wheat.

INTRODUCTION

The 1RS.1BL translocation chromosome was one of the earliest of so-called alien chromatin additions into wheat and is generally considered to be associated with the disease resistance (Zeller, 1973) and a step-change in yield achieved with the release of the Veery lines by CIMMYT (Rajaram et al., 1983). A survey by R Schlegel showed that approximately 30% of wheat cultivars released after the year 2000 carry the 1RS.1BL translocation (http://www.rye-gene-map.de/ rye-introgression/) (Schlegel and Korzun, 1997). The *Lr26*, *Sr31*, *Yr9*, *Sr50* rust resistance genes and the powdery mildew, *Mlg* locus have been identified on 1RS.1BL chromosomes as well as genetic factors affecting root biomass (Mago et al., 2002 and 2015; Ehdaie et al., 2003; Waines and Ehdaie, 2007; Sharma et al., 2011). The grain yield associated with 1RS.1BL has been shown to be disrupted by 1RS-1BS recombinants in the terminal region of 1RS as characterized in field trials of wheat accessions carrying these

recombinants in the same genetic background (Lukaszewski et al., 2000; Howell et al., 2014 and 2019). The 1RS.1BL chromosome has also been factored into maintaining male sterility in hybrid wheat programs (Lukaszewski et al., 2017).

The 1RS rye chromosome segment in wheat varieties has at least 3 sources, namely, as 1RS.1BL in *Triticum aestivum* cv Salmon (Japan), as 1RS.1BL in *T. aestivum* varieties originating from Germany and as 1RS.1AL in *T. aestivum* cv Amigo from the USA (Schlegel and Korzun, 1997). The 1RS.1BL translocation has been widely introduced into wheat cultivars globally for conferring a broad-range of resistance to races of powdery mildew and rusts, environmental adaptability and yield performance (Zeller, 1973; Rajaram et al., 1983; Schlegel and Korzun, 1997; Bartoš and Bareš, 1971; Sukumaran et al., 2015).

At a structure level, 1RS.1BL was one of the early chromosomes to have specific DNA sequences assigned to it through the analysis of chromosomes using inbred lines of rye to facilitate locating molecular markers and agronomic traits to 1RS as well as the entire rye genome (Lawrence and Appels, 1986; Miedaner et al., 2012; Bauer et al., 2016). *In situ* hybridization technology with labelled sequenced probes has allowed the convenient microscopic visualization and identification of translocations involving 1RS (Appels et al., 1978; McIntyre et al., 1990; Liu et al., 2017).

The favorable agronomic features have been a significant driver for sequencing the 1RS.1BL chromosome in the China wheat cultivar, AK58. In the available rye genome data from an inbred rye line 27,784 gene models (and segments) were sourced for assigning gene models to the 1RS segment and these generally fell within gene models aligned from the wheat reference genome sequence (Bauer et al., 2016; IWGSC et al., 2018). This study provides the linear genome level structure of AK58-1RS.1BL utilizing a combination of Illumina and PacBio sequencing with de novo NR Magic for the initial assembly followed by HiC scaffolding and alignment to high density molecular genetic maps to generate the final assembly. The genome structure identified new gene models, several multi-gene families

84 likely to be involved in yield attributes associated with 1RS.1BL and resolved gene families
85 involved in disease resistance and other agronomic traits.

86 **RESULTS**

87 **Assembly of the 1RS.1BL genome of wheat cv AK58**

88 The details of the assembly are provided in Figure S1 and Methods, and include the de novo
89 NR Magic software to carry out a primary alignment into contigs, followed by the HiC
90 process for scaffolding the contigs. Finally, we generated a high-quality chromosome-scale
91 assembly of 1RS.1BL translocation with a total length of 748,715,293 bp and predicted 4,996
92 genes using four different annotation pipelines and alignment with the IWGSC RefSeq v1.0
93 annotation. The alignment of our AK58_chr1RS.1BL_v6 to the reference Chinese Spring (CS)
94 1B is shown in Figure 1a. The AK58_chr1RS.1BL_v6 assembly was examined in detail in the
95 terminal 22 Mb region because, in general, this region of wheat genome assemblies can be
96 problematical with respect to contig orientation. The assembly shown was the best alignment to
97 available genetic mapping information for 1RS.1BL, as shown in Figure 1b (Mago et al., 2002;
98 Howell et al., 2014; Sharma et al., 2009), using the markers, gamma secalin (8.82 Mb) and
99 BE444266 (24.41 Mb). The IB267 (0.815 Mb) and iag95 (3.92 Mb) markers were located
100 following discussions with J Dubcovsky (pers. comm., see Figure 1b).

101 **Alignment and *in situ* cross-referencing of the AK58-1RS.1BL genome**

102 The *in situ* probes are generally repetitive and although the number of repeats was clearly
103 collapsed during the assembly process, all the regions aligned by *in situ* hybridization using
104 double labelling could be assigned positions in the new assembly (McIntyre et al., 1990; Liu
105 et al., 2017; Zhang et al., 2004). Importantly the macro-level structure of 1RS.1BL could be
106 validated in this way (Figure 1c). The repetitive array of Sc119.2 sequences at 117.6 Mb (31
107 copies of the core 45 bp repeat unit) on 1RS were under-represented in the assembly, relative
108 to the array at 0.4 Mb (662, 45 bp repeat units) based on comparing the *in situ* hybridization
109 signals which indicated qualitatively similar signals (Figure 1c). The amplification of
110 repetitive gene families in 1RS (Sc119.2, Sc200) in positions that were not in a syntenic order
111 has occurred against a background of a conserved syntenic order of high confidence (HC)

112 gene models (Figure 1a). The repetitive gamma-secalin and omega-secalin gene families were
113 located in syntenic positions relative to 1BS of CS. In Figure 1d, a portion of a diversity
114 analysis is shown using a 660K SNP-chip for SNPs that could be clearly scored in 36 1RS
115 containing lines (identified using the gamma-secalin based PCR probes) (Figure S2 and Table
116 S1). A subset of 9 wheat lines are shown for comparison to confirm that at the macro-level the
117 1RS is a large haplotype block, as described by Cheng et al. (Cheng et al., 2019). At a
118 micro-level at least 6 groups, or haplotypes, of 1RS.1BL could be identified using the
119 AK58-1RS as a reference, and these are accounted for by considering the different rye
120 genome sources used in the intense breeding efforts in China combining 1RS.1BL containing
121 wheat lines in crosses with triticales, rye and alternative sources of 1RS.1BL (Figure 1d,
122 Figure S2 and Table S1). The 1RS in AK58 groups with only 3 other 1RS lines.

123 In our assembly, the size of 1RS is 275 Mb, 28% larger than 1BS (215 Mb) and is consistent
124 with the overall genome size of rye (7-8 Gb) being approximately one-third larger than the
125 diploid genome of barley or wheat progenitors. A comparison of the TE-complement between
126 1RS, 1AS, and 1DS in AK58 and 1BS in CS indicated that 12 TE subfamilies (Figure S3 and
127 Table S2) were dominant in 1RS with a total length in excess of 41.9 Mb (15.27% of the 1RS
128 length), compared to only 4.9 Mb in 1AS, 3.5 Mb in 1DS and 4.8 Mb in 1BS of CS. The 12
129 rye dominant TE included nine LTRs. There were five TE families, *LTR-Gypsy-RLG_famc9.2,*
130 *LTR-RLX_famc7, LTR-RLX famc21, Unknown-XXX_famc9,* and *Unknown-XXX_famc81,* in
131 which the length ratios of 1RS/1AS, 1RS/1BS and 1RS/1DS are range from 4 to 203 (Table
132 S2). Although most of the rye dominant TEs were distributed in 1RS, including gene-flanking
133 regions, some were more prominent in the centromere region (LTR-Gypsy-RLG_famc36,
134 Figure S3; see also centromere section below).

135 **Centromere structure at the 1RS-1BL boundary**

136 The availability of a rye centromere sequence (pAWRC, Francki, 2001) that could be
137 distinguished from the wheat centromere repeats, CRWs, allowed a more detailed analysis of
138 the rye-wheat hybrid centromere region. A 800 bp region from pAWRC (AF245032) that had
139 no similarity to CRWs was used to define a 9.9 Mb region on the 1RS side of the 1RS.1BL

140 centromere while CRW/CCS1 (AB048244.1, a 249 bp repetitive unit), and Tail 1 (AB016967)
141 from the wheat centromere were used to define the 1BL side of the 1RS.1BL chromosome
142 (Figure 2a) (Francki, 2001; Keeble- Gagnère et al., 2018). In total the region covered by these
143 centromere markers was 10.87 Mb within a region of 272.02 Mb to 296.20 Mb (24.18 Mb).
144 The centromere marker sequences are evident in the matrix analysis (Figure 2a) as large arrays
145 of repetitive sequences. At the junction between 1RS and 1BL, to form the 1RS.1BL
146 chromosome, there exists a sharp change-over from the blocks of repetitive sequences carrying
147 pAWRC (Figure 2a-a1, blue dashed line box) to the CRW markers sequences (Figure 2a-a1,
148 red dashed line boxes). The matrix defines the junction between 281.93 Mb and 281.99 Mb
149 and is between a RLG_Taes_Abia_B_3Brph7-445 element (coordinates 281,918,330 to
150 281,927,173 bp) and a LTR, Gypsy; consensus sequence (coordinates 281,926,633 to
151 281,935,207 bp) using TREP database (http://botserv2.uzh.ch/kelldata/trep-db/) to identify the
152 LTR elements. The junction can be most easily modeled as resulting from a recombination
153 event involving an Abia sequence located in Abia-like segments within CRW/Cereba elements
154 in the wheat centromere and an Abia element in the original 1R chromosome.

155 The ca 150 Mb region that is relatively poor in annotated gene models (coordinates 165 to
156 313 Mb, Figure 1a and Figure 2a, dashed line boxes) houses predicted genes that code for
157 peptides less than 50 amino acids and has a good coverage of hits from RNA-seq data
158 originating from a range of tissues that could not be clearly assigned to gene models.
159 Immunoprecipitation of CENH3 binding genome sequences from CS and AK58 nuclei
160 provided a class of sequence to further define the core 31 Mb centromere region more clearly.
161 The CS-CENH3 sequences differentiated the wheat centromere segment on 1BL from 1RS
162 when aligned across the AK58_chr1RS.1BL_v6 assembly (Figure 2a-a2, coordinates 282 to
163 292 Mb) and also identified two sections of non-centromere (wheat) DNA (blue solid line
164 boxes in Figure 2a-a5) even though the well-known centromere transposable elements,
165 Cereba and Quinta, exist in these regions (Figure 2a-a1 and Figure 2a-a4). The AK58-CENH3
166 sequences mainly identified the rye centromere segment 272 to 282 Mb on 1RS (Figure
167 2a-a3). The dot matrix of CS vs AK58 core centromere sequences (Figure 2a-a5) indicated a
168 region where the two genomes are structurally rearranged relative to each other.

169 The *in situ* localization of the centromere Abia (rye) and CRW (wheat) sequences as well as
170 the CENH3 protein using fluorescent antibodies (Figure 2b) indicated that the AK58 CENH3
171 sequences mainly co-located with the Bilby sequences (rye, Abia TE family) and confirmed
172 that the CENH3-ChIP protocols selected specific sub-populations centromere sequences.

173 **Expression of 1RS genes in a wheat background**

174 Transferring alien chromosome or chromosomal fragments from wheat relatives to wheat is
175 an efficient approach for wheat improvement, relying on the expression of the alien
176 chromosome genes in a wheat background. There are 1,480 high confidence genes annotated
177 in 1RS and 1,560 on 1BS in CS (tissue expression summarized in Figure 3a) and entries of
178 particular interest relate to the deployment of the 1RS.1BL chromosome in wheat breeding
179 with a focus on those affecting grain quality and yield gains. Our study using the RNAseq
180 data sets indicated that the 1RS gene expression is generally successful in wheat backgrounds
181 and that 1RS genes do not interfere with wheat gene expression in total. A graphical
182 representation of tissue-based expression groups is summarized in Figure 3a and 3b for AK58
183 and CS. At this broad level it is evident that 1RS has a greater percentage of genes expressed
184 specifically in the grain tissue relative to CS (Figure 3b). In Figure 3c, the tissue specific gene
185 expression patterns among the AK58 and CS chromosome 1 pairs are compared in more detail
186 and it is evident that only 1BS in AK58 (= 1RS), has higher levels than 1BS of CS at the
187 grain-20 DPA stage, where we found 6.44× higher levels of total gene expression in 1RS of
188 AK58 relative to 1BS in CS. This grain-20 DPA stage is the active grain filling stage and the
189 higher levels of gene expression may thus relate to the large grain size (45 g/1000 grain) and
190 higher yield (7.5 t/h) of AK58 compared to the small grain size (35 g/1000 grain) and lower
191 yield (3.0 t/h) of CS.

192 The hierarchical clustering of gene expression in Figure S4a within the AK58-1RS gene space
193 of the developing grain provides a greater resolution the view of the gene families during the
194 progressive differentiation of the grain tissue occurs as the spike matures and was consistent
195 with IWGSC (IWGSC et al., 2018) and Ramírez-González (Ramírez-González et al., 2018).
196 In Figure S4b, the early, prominent, expression of the MIKC-type MADS-box transcription

197 factor family was striking. Genes that were highly expressed in grain tissue were of interest
198 because historically the presence of 1RS in bread wheat was considered detrimental for
199 qualities relating to the performance of flour from these wheat lines in the standard processing
200 methodologies (Lukaszewski et al., 2000; Gobaa et al., 2007; Li et al., 2016). Transcription
201 factor gene families prominently expressed in roots (as well as leaves) such as Cys3His zinc
202 finger protein (C3H), MYB protein family (MYB) and WRKY signature containing
203 transcription factor (WRKY) (Figure S4b) were of interest because this class of gene was well
204 represented in the region that was studied by Howell et al. in which disruption of the genome
205 structure through recombination with wheat 1BS reduced yield (more detailed analysis below)
206 (Howell et al., 2019).

207 **The pentatricopeptide-repeat (PPR) gene family at the *rf*/*Rf* ^{multi} loci of 1RS and 1BS**

208 PPR domain carrying proteins form the one of largest gene families of land plants and are
209 involved in the regulation of RNA metabolism including RNA editing, stability, processing,
210 and splicing to translation (Lurin et al., 2004; Cheng et al., 2016). Most of restorer of fertility
211 (*Rf*) genes cloned in model organisms encode P-class PPR proteins. AK58 is a 1RS.1BL
212 variety and the 1RS.1BL translocation replaces *Rf* ^{multi} locus from chromosome 1BS of wheat
213 (15.28 to 59.84 Mb in CS) in multiple CMS systems (*Aegilops kotschyi, Ae. uniaristata* and
214 *Ae. mutica*) to generate male sterile wheats (Tables S3 and 4) (Lukaszewski et al., 2017;
215 Tsunewaki, 2015). The syntenic region in AK58-1RS is at 0.58 to 52.35 Mb in our assembly
216 (Tables S5 and 6). The overall gene numbers in the regions that satisfy the definition of the
217 PPR gene models are 21 in CS and 8 in AK58(Tables S3-5). A cluster of 11 PPR-family
218 genes in CS-*Rf* ^{multi} are a tandem array (at location 56.49 to 58.34 Mb) and a similar cluster
219 exists in AK58-*rf* ^{multi} (at 48.60 to 49.42 Mb) but is not in an exactly matching syntenic
220 location (Figure 4a, Tables S6 and 7). One gene model, *TraesCS1B01G072900*, from the CS
221 cluster has a homologous sequence *TraesAK58CH1B01G045250* at 49.41 Mb in AK58 and
222 this gene in AK58 is also syntenic to *TraesCS1B01G074600* in CS-*Rf* ^{multi}. The
223 *TraesCS1B01G074600* gene is, in turn, syntenic to another AK58 gene
224 (*TraesAK58CH1B01G043900*) in the AK58-*rf* ^{multi} region, so we consider it useful to define
225 this as one closely related group represented by *TraesCS1B01G072900*. These relationships

226 reflect a complex micro-level relationship between the AK58- *rf* ^{multi} and CS-*Rf* ^{multi} regions
227 which results in the different expression patterns that are relevant to the male
228 fertility/restoration of fertility (Figure 4b). The three P-class proteins from the CS-*Rf* ^{multi}
229 region, namely, *TraesCS1B01G072300*, *TraesCS1B01G072900* and *TraesCS1B01G074600,*
230 and their 1RS homologs, have significant mitochondrial targeting scores (Figure 4c, Tables S6
231 and 8) and between these genes only *TraesCS1B01G072300* shows the most striking
232 difference in transcription in FM tissue when compared to its homolog in AK58
233 (*TraesAK58CH1B01G045100*) (Figure 4b).

234 Taken together, the CS-*Rf* ^{multi} /AK58-*rf* ^{multi} comparison suggests the *TraesCS1B01G072300*
235 and *TraesCS1B01G072900* are the most likely candidate genes of the multi fertility restoring
236 locus *Rf* ^{multi} in the context of the 1RS.1BL translocation replacing the *Rf* ^{multi} locus from
237 chromosome 1BS in multiple *Aegilops* CMS systems that generate male sterile wheats and
238 male fertility being subsequently restored by the 1BS-*Rf* ^{multi} locus (Lukaszewski et al., 2017;
239 Tsunewaki, 2015).

240 **The grain storage protein gene families**

241 Gamma and omega secalin sequences were identified and aligned to gamma and omega
242 gliadins from the CS chromosome 1B. While the sequence similarity between gamma gliadins
243 and gamma secalins was over 70%, omega gliadin and omega secalin sequences differed
244 significantly both in the signal peptide as well as in their repetitive regions. Nineteen gamma
245 secalin coding sequences were identified from which 18 were located in a single cluster at
246 1RS between positions 8,722,719 bp and 8,904,808 bp (Figure 5a). Using an extensive
247 proteome database of rye grain peptides (Figure S1 and Methods) (Bose et al., 2019), half of
248 these genes were verified at peptide level as bone-fide gamma secalin protein coding genes.
249 Eight sequences (7 gamma secalins, 1 purinin) represented complete sequences, two
250 sequences were partial sequences and ten sequences contained frameshifts or internal stop
251 codons. Similarly, a cluster of 18 omega secalin genes were identified, between positions
252 18,457,234 bp and 18,690,191 bp with 13 verified at the proteome level (Figure 5b). Between
253 the gamma secalin and omega secalin loci a single purinin gene was identified in a conserved

254 position compared to chromosome 1B.

255 Within the identified gamma secalins there were two sequences (Gamma secalin 5 and
256 Gamma secalin 16) with Tryp_alpha_amyl domain (PF00234) while the majority of gamma
257 secalins possess a single Gliadin Pfam domain (PF13016). In bread wheat, all the identified
258 gamma gliadins and low molecular weight (LMW) glutenins have PF13016 (Gliadin)
259 domains, and Tryp_alpha_amyl domains were only found in alpha gliadins among the gliadin
260 and glutenin types. The Pfam domain composition of available secalin sequences from
261 UniProt DB indicates the Gliadin domain (PF13016) and Tryp_alpha_amyl domain (PF00234)
262 are both characteristic of rye secalins, while PF00234 domains were only identified in the 75
263 k gamma secalins. The Tryp_alpha_amyl domain containing proteins represent a sulphur-rich
264 domain structure and are primarily characterized to have functions related to defense
265 mechanisms against pathogens or lipid transport (non-specific lipid transfer proteins). As both
266 in 1BS and 1RS the major storage proteins are located within regions enriched in disease
267 resistance proteins this might indicate a potential alternative function of these proteins and
268 their possible involvement in stress responses.

269 There were eleven nsLTP genes found on the 1RS chromosome arm, ten of which represented
270 the PR60 nsLTP sub-type (UniRef100_B2C4K0) clustered between 56.6 Mb and 57.2 Mb and
271 specifically expressed in grain tissue (Figure 5c); a single nsLTP (at 42.24 Mb) was highly
272 expressed in roots. On the long arm, 7 nsLTPs, 5 LTPs and 4 LTP-like sequences were
273 identified from which 3 short LTP-like sequences were grain specific. All the prolamin genes
274 present on 1RS were specifically/preferentially expressed in the grain, while the nsLTPs were
275 also expressed in other tissues such as under-spike internodes and young spikes.

276 **The disease resistance gene families**

277 The *Pm8* gene, orthologue of the *Pm3*, provided a good model for the RGA gene in the region
278 although the expression of the gene itself was not confined to any single tissue category
279 (Hurni et al., 2013). The identification of *Pm8* suggested that 1RS of AK58 is from diploid
280 rye Petkus. The RGA genes specifically expressed in different tissue were assessed against a

281 total of 2,871 gene models with the NB-ARC domain in their structure were identified within
282 the IWGSC RefSeq v1.0. In the AK58 1RS.1BL chromosome, disease resistance gene models
283 were identified (Table 1, Figure S1 and Methods). The NB-ARC domains are the most
284 common feature within disease resistance genes and are key components of apoptosomes that
285 are involved in recognizing the presence of a pathogen or DNA damage in the cell and
286 responding to the problem by localized cell death to protect the organism per se
287 (Crespo-Herrera et al., 2017; Li et al., 2016). The range of gene diversity is consistent with
288 the range of intrinsic and extrinsic stimuli to which wheat is exposed. Among the 22
289 1RS-specific gene models we identified three broad categories, dominated by a large group
290 (15) which comprised members of RGA families located on wheat 1B as well as other
291 chromosomes and included genes that were identified as having disease resistance-like
292 protein and tyrosine kinase domains (Table S9). Four gene models were part of a very large
293 family encoding proteins with lrr-serine/threonine kinase domains. Three gene models were
294 of particular interest in that they were absent from 1BS and thus represent novel resistance
295 genes introduced by 1RS (details in Table S9). Two of these gene models
296 *TraesAK58CH1B01G008800* (at 4,676,665 bp) and *TraesAK58CH1B01G010100* (at
297 6,010,958 bp) are closely linked to, and on the proximal side of, the marker BE405749.1
298 which defines a region housing *Lr26* (Mago et al., 2002), as well as having the protein fold
299 c6j5tc associated with the disease resistance gene rpp13-like protein 4, determined using
300 Phyre2 (Kelley et al., 2015).

301 **Characterization of the 1RS region disrupted by recombination between 1RS and 1BS**

302 The yield-related region (YR) comprised the genome region in the terminal 14 Mb on the
303 1RS.1BL chromosome based on published molecular marker evidence in Mago et al. and
304 Howell et al. (Mago et al., 2002; Howell et al., 2014). The region exists within the terminal 22
305 Mb and housed 259 genes, from a total of 465, that could be characterized by the clusters of
306 co-expression representing gene networks potentially disrupted by recombination events
307 between 1RS and 1BS. The analysis in Figure 6 shows the co-expression matrix of the
308 contig-356, -445, -624 and -517 1RS genes (Table S10). The gene expression was calculated
309 using the Morpheus analysis tool (https://software.broadinstitute.org/morpheus/) and a 0.5

310 FPKM cut-off. The co-expression similarity matrix was calculated using Pearson correlation
311 and the clustering was carried out using only the co-expression values > absolute value 0.7
312 FPKM as being significant (highlighted red = positively correlated, blue = negatively
313 correlated). The contigs annotated as "Tissues" were identified based on the stage and
314 tissue-specific clustering in Figure 6. The boxed regions identified gene clusters that formed
315 qualitatively major networks based on shared patterns of expression. The 1RS genes in
316 clusters 1-7 shown in Figure 6 are combinations of models that are tissue specific in
317 expression and ones that are more generally expressed and overall, the analysis indicates that
318 the genes in the YR region are widely networked to genes involved in a broad range of
319 biological activity with a particular focus on root specific genes (Table S10). The clusters also
320 include genes potentially interacting with nitrogen metabolism related genes as well as genes
321 involved in stress responses and adaptation and thus a disruption in the activity profiles is
322 predicted to have wide ranging effects on a complex phenotype such yield. In particular we
323 identified TraesAK58CH1B01G010700 (formin-like domain protein) and
324 TraesAK58CH1B01G007500 (Cathepsin-L, homolog) genes as having the highest number of
325 co-expression partners. The rice homolog for the *TraesAK58CH1B01G010700* gene is
326 *Os05t0104000-00*, a formin-like-domain protein FH14, and defines a class of protein which
327 interacts with microtubules and microfilaments to regulate cell division. This gene also shows
328 co-expression with a nitrate reductase at chromosome 6B. The *TraesAK58CH1B01G010700*
329 gene showed a broad co-expression-based network including interactions with auxin response
330 factors on chromosomes 1A, 1B, 1D, 2B, 5A, 7A, 7B, 7D.

331 **DISCUSSION**

332 Our study provides the genome assembly for chromosome 1RS.1BL, a chromosome which
333 was one of the early successes of genetic engineering at a chromosome level that has had a
334 significant impact on wheat yield and hence food production globally (Schlegel and Korzun,
335 1997). The value of our assembly is demonstrated through the identification of 1RS-specific
336 genes within an overall gene space that showed excellent synteny with 1BS from wheat. In
337 contrast the non-gene space is shown to have regions of highly amplified, relatively short
338 (100 – 500 bp), units of DNA sequences in regions which are not syntenic to equivalent

339 regions in 1BS and are suggested to be possible sites for recombination type events between
340 1R and 1B. The detailed analysis of the centromere identified the junction between 1RS and
341 1BL and this was found to comprise part of an Abia transposable element (TE) on the 1RS
342 side and a Cerebra TE on the 1BS side suggesting that a recombination event between the
343 arrays of Abia TEs that characterize the rye centromere and the arrays of Cereba TEs in the 1B
344 centromere, which can also carry Abia-like sequences (http://botserv2.uzh.ch/kelldata/trep-db/),
345 could have generated the 1RS.1BL chromosome (Francki, 2001). Our analysis of the CENH3
346 locations indicated a shift in the location of the centromere assembly defined by CENH3 to the
347 rye side of the translocation and provided a clear indication of mobility in the location of the
348 point of attachment of micro-fibrils for mitosis.

349 Specific families of gene models characterized in detail in this study included the genes
350 predicted to be involved in the male sterile/male fertility restoration interactions, resistance
351 gene analogs and the gamma and omega secalin storage proteins. The substitution of 1BS
352 with 1RS in 1RS.1BL wheat lines results in the replacement of three PPR proteins that have
353 high mitochondria target scores. In the context of the CS-Rf^{multi}/AK58-rf^{multi} comparison
354 carried out, it is suggested that *TraesCS1B01G072300* and *TraesCS1B01G072900* are
355 representative of the most likely candidate genes of the multi fertility restoring Rf^{multi} locus
356 because they show the most striking differences in transcription to its AK58 homolog and
357 could thus be most significant in restoring male fertility the 1BS-Rf^{multi} locus in the multiple
358 CMS systems-male sterile wheats where 1RS.1BL translocation replaces the Rf^{multi} locus
359 from chromosome 1BS (Lukaszewski et al., 2017; Tsunewaki, 2015). Our analysis of the
360 resistance gene analogs identified three genes that were absent from 1BS and thus represent
361 new resistance genes for varieties carrying the 1RS.1BL translocation. Two of these genes,
362 *TraesAK58CH1B01G008800* (at 4,676,665 bp) and *TraesAK58CH1B01T0G0100* (at
363 6,010,958 bp), locate in the genome region housing genetically defined disease resistance
364 genes and are thus candidate genes for entities such as *Lr26*.

365 The substitution of 1BS in 1RS.1BL wheat lines also results in the replacement of a major
366 source of wheat gliadin proteins on 1BS with secalin protein coding genes on the 1RS.1BL

367 chromosome. The analysis of the gamma and omega secalin storage protein coding regions
368 and expression identified pseudogenes as well as two sequences (Gamma secalin 5 and
369 Gamma secalin 16) with Tryp_alpha_amyl domain (PF00234). The Tryp_alpha_amyl domain
370 containing proteins, represent a sulphur-rich domain structure are more broadly associated
371 with defense mechanisms against pathogens, lipid transport and storage function and suggests
372 an involvement in stress responses. In the context of unwanted processing attributes ("sticky"
373 dough) associated with flour from 1RS.1BL containing wheat cultivars genes related to the
374 production of xylose and arabinoxylose and the xylanase domain protein
375 (TraesAK58CH1B01G088700) specifically expressed at 4 DPA in the grain could be related to
376 the moderation of arabinoxylans that may be associated with increased water absorption
377 resulting in the "sticky" dough defect (Gobaa et al., 2007; Henry et al., 1989; Lee et al., 1995).

378 The mapping of published DNA probes to the 1RS assembly indicated that a 9 Mb region (in
379 the terminal 14 Mb, "YR" region) was disrupted by the 1RS/1BS recombinants selected by
380 Lukaszewski (Lukaszewski et al., 2000). The genes in this region are widely networked, as
381 expected, based on co-expression analyses and have a striking representation of root-specific
382 genes that are good candidates for relating the changes in root phenotype to the disruption of
383 the 9Mb region defined by Howell et al (Howell et al., 2014 and 2019). Our study highlighted
384 the complex negative and positive interactions among the genes in this YR region and
385 identified TraesAK58CH1B01G010700 (formin-like domain protein) and
386 TraesAK58CH1B01G007500 (Cathepsin-L, homolog) genes as having the highest number of
387 co-expression partners. The rice homolog for the *TraesAK58CH1B01G010700* gene is
388 *Os05t0104000-00*, a formin-like-domain protein FH14, showed a broad co-expression-based
389 network across 8 chromosomes consistent with a gene model that encodes a protein regulating
390 cell division.

391 In brief, we generated a high quality 1RS.1BL translocation chromosome sequence which
392 provided a basis for defining gene underpinning the agronomic attributes of the 1RS.1BL
393 translocation chromosome in wheat improvement. The structure, gene complement of
394 1RS.1BL and candidate genes identified in this study provides the resource-of-choice for

395 refining the contribution of this chromosome to wheat genetic improvement.

396 **EXPERIMENTAL PROCEDURES**

397 **Gene annotation**

398 Protein-coding identification and gene prediction were carried out using a combination of
399 homology-based prediction, *de novo* prediction, and transcriptome-based prediction methods
400 (Figure S1). Five *ab initio* gene prediction programs, Augustus (v.2.5.5), Genscan (v.1.0),
401 GlimmerHMM (v.3.0.1), Geneid, and SNAP, were used to predict coding regions in the
402 repeat-masked genome. Proteins from ten plant genomes (*T. aestivum*, *T. turgidum dicoccides,*
403 *T. urartu*, *Ae. tauschii*, *Hordeum vulgare*, *Brachypodium distachyon*, *Oryza. sativa*, *Zea mays*,
404 *Sorghum bicolor* and *Setaria italic*) were downloaded from EnsemblPlants
405 (http://plants.ensembl.org/index.html). *Panicum virgatum* genome was downloaded from
406 Phytozome (https://phytozome.jgi.doe.gov/pz/portal.html). Protein sequences from these
407 genomes were aligned to the AK58 assembly using TblastN with an *E-value* cutoff of 1e-5.
408 The BLAST hits were conjoined using Solar software. GeneWise was used to predict the
409 exact gene structure of the corresponding genomic regions for each BLAST hit. Homology
410 predictions were split into two sets, which included a high-confidence homology set
411 (HCH-set) with predictions from genomes with CS wheat and a low confidence homology set
412 (LCH-set).

413 A collection of wheat FLcDNAs (16,807 sequences) were directly mapped to the AK58
414 genome and assembled by Program to Assemble Spliced Alignments (PASA). Gene models
415 created by PASA were denoted as the PASA-FLC-set (PASA full length cDNA set), this gene
416 set was used to train the *ab initio* gene prediction programs. RNA-seq data were mapped to
417 the assembly using Tophat (v.2.0.8). Cufflinks (v.2.1.1) was then used to assemble the
418 transcripts into gene models (Cufflinks-set). In addition, a total of 2,016 Gb RNA-seq data
419 from different organs (root, leaf, internode, flower and developing seed) were assembled by
420 Trinity, creating several pseudo-ESTs. These pseudo-ESTs were also mapped to the AK58
421 assembly and gene models were predicted using the PASA. This gene set was denoted as
422 PASA-T-set (PASA Trinity set).

423 Gene model evidence from the HCH-set, LCH-set, PASA-FLC-set, Cufflinks-set, PASA-T-set
424 and *ab initio* programs were combined by EvidenceModeler (EVM) into a non-redundant set
425 of gene structures. Weights for each type of evidence were set as follows: HCH-set >
426 PASA-FLC-set > PASA-T-set > Cufflinks-set > LCH-set > Augustus > GeneID = SNAP =
427 GlimmerHMM = Genscan. Gene model output by EVM with low confidence scores was
428 filtered using: (1) coding region lengths of 150 bp, and (2) supported only by *ab initio*
429 methods and with FPKM<1.

430 In an approach similar to that described for *Gossypium raimondii* genome studies (Yan et al.,
431 2016), we further filtered gene models based on Cscore (Cscore is a peptide BLASTP score
432 ratio mutual best hits BLASTP score), peptide coverage (coverage is highest percentage of
433 peptide aligned to the best of homologues) and overlap of its CDS with TEs. The Cscore and
434 peptide coverage were calculated as described in *G. raimondii* (Yan et al., 2016). Only
435 transcripts with a Cscore ≥ 0.5 and peptide coverage ≥ 0.5 were retained. For gene models
436 with more than 20% of their CDS sharing an overlap with TEs, we required that its Cscore
437 must be at least 0.8 and that its peptide coverage must be at least 80%. Finally, we also
438 filtered out gene models of which more than 30% of the peptides in length could be annotated
439 as Pfam or Interprot TE domains.

440 **Transcript analysis**

441 Two transcriptome datasets derived from AK58 genome sequencing project were used for this
442 analysis. (1) 42 diverse samples (each 3 biological replicates, total 126 libraries) were
443 collected for AK58, covering anther development to the tetrad stages, floret/spikelet meristem,
444 three stages of stem development, three stages for flag leaf, five stages of grain development,
445 and 7 day seedling for the leaf and root sample under normal or six abiotic stresses conditions.
446 (2) Seven tissues shared between AK58 and CS (each 3 biological replicates, total 42
447 libraries), covering 21 days seedling for the leaf and root, floret meristems stage, and four
448 grain development stages (4/10/15/20 days after flowering).

449 To align RNA-seq sequences to the genome assembly, the BLAT software within Apollo was
450 used in two modes (Lee et al., 2013), one allowing only perfect matches and a second mode
451 using the Hi-sat-2 default settings (https://ccb.jhu.edu/software/hisat2/index.shtml) equating
452 to approximately 80% similarity over at least 80% of the sequence. Only unique gene models
453 were used to define the 1RS.1BL synteny.

454 Gene co-expression matrix of the contig-356, -445, -624 and -517 1RS genes were developed
455 using the Morpheus matrix visualization and analysis tool
456 (https://software.broadinstitute.org/morpheus/). Mean values of gene expression data obtained
457 from the different tissue samples with a 0.5 FPKM cut-off were used to calculate Pearson
458 correlation coefficients. The obtained similarity matrix was used for hierarchical clustering
459 with complete linkage. Rows and columns represent the individual gene models present in the
460 analyses 22 Mb region (Table S10). Tissue specific expression patterns and location within the
461 analyzed region are annotated by different colors were obtained from the analysis presented in
462 Figure 6. Co-expression similarity values > absolute value 0.7 FPKM as being significant are
463 highlighted in red (positively correlated) and blue (negatively correlated).

464 **Chromosome preparation**

465 The protocol for root tip mitotic metaphase chromosomes of AK58 was largely referred to the
466 previously report (Han et al., 2006). Briefly, the roots of AK58 grew to 1.5-2.0 cm in length
467 were excised and treated with nitrous oxide gas for 2 h under pressure under 1 MPa. The
468 treated roots were fixed in ice-cold 90% acetic acid for 10 min. Subsequently, the root tips
469 were dissected and digested by 2% cellulose Onozuka R-10 (Yakult Pharmaceutical, Japan)
470 and 1% pectolyase Y23 (Yakult Pharmaceutical) solution for 45 min at 37°C. After digestion,
471 the root sections were broken in a 90% acetic acid. The cell suspension was dropped and
472 air-dried on glass slides for chromosome observation.

473 **Fluorescence *in situ* hybridization**

474 The method of sequential FISH and Non-denaturing FISH (ND-FISH) with different labeled
475 probes for karyotype analysis of AK58 was mainly performed according to the previously

476 published protocol (Fu et al., 2015). The probe Sec1 for rye specific secalin was labeled with
477 Texas Red-5-dUTP (Invitrogen) or Alexa Fluor 488-5- dUTP (Invitrogen) using nick
478 translation for FISH (Clarke et al., 1996). The oligonucleotide probes for ND-FISH with
479 centromeric specific probe CCS1, 18S-45SrDNA probe pTa71, and probe pSc119.2 were
480 referred to Tang et al. (Tang et al., 2014). The repeats probes pSc200 and 5SrDNA were from
481 the previously published information (Fu et al., 2015; Lang et al., 2019). The synthetic oligo
482 probes were 5' end-labeled with 6-carboxyfluorescein (FAM) for the green signal and
483 6-carboxytetramethylrhodamine (Tamra) for the red signal. The slides after FISH and
484 ND-FISH were mounted with Vectashield mounting medium containing 1.5 μg/mL 4, 6 -
485 diamidino -2- phenylindole (DAPI, Vector Laboratories, Burlingame, CA, USA). The FISH
486 images were captured with an Olympus BX-53 microscope equipped with a DP-80 CCD
487 camera.

488 **660K SNP Analysis of the 1RS Lines and Non-1RS Lines**

489 Wheat 660K SNP Array designed by the Institute of Crop Sciences of the Chinese Academy
490 of Agricultural Sciences and synthesized by Affymetrix® was applied to genotype 36
491 1RS.1BL lines and 9 non 1RS.1BL lines. All the SNPs were merged to FASTA file for 45
492 samples. TreeBeST (1.9.2) (http://treesoft.sourceforge.net/treebest.shtml#intro) nj was used to
493 build neighbor-joining phylogenetic tree with parameters: "-b 1000" and MEGA7 was used to
494 visualize phylogenetic trees (Kumar et al., 2016).

495 **ChIP-seq**

496 We used chromatin immunoprecipitation and sequencing technique to find the centromeric
497 DNA by CENH3 antibody, which was a rabbit polyclonal antiserum and was raised against the
498 peptide 'CARTKHPAVRKTK' (Li et al., 2013). ChIP was conducted using young leaves of
499 AK58 as previously described (Nagaki et al., 2003). The enriched DNA samples were
500 sequenced using Illumina Hiseq X-10 to generate 150 bp paired-end sequences. Reads were
501 filtered with TrimGalore (http://www.bioinformatics.babraham.ac.uk/projects/trim_galore/)
502 and aligned to the AK58 genome sequence using Bowtie 2 (Langmead and Salzberg, 2012). We
503 only retained reads that determined the unique position, which MAPQ >= 30, for further

504 analysis. The distribution of ChIP-seq reads were calculated using the unique read number per 1
505 kb window. ChIP-Seq data precipitated from CS in our previous study (SAMN11655702) were
506 analyzed as parallel.

507 **Centromeric sequence analysis**

508 In order to detect the sequence variation, we aligned the sequence of 1B from CS to AK58
509 genome using NUCmer program (parameter: -c 700) in MUMmer4 package (Marcais et al.,
510 2018). We used mummerplot program in the same software to draw 245–315 Mb of 1B
511 chromosome from AK58. Consensus of *CRW*, *Quinta* and *Bilby* were aligned to AK58
512 genome and calculated the percentage per 50 kb to reveal the sequence composition.

513 **Immuno-co-localization Analysis of CENH3 with *CRW* and *Bilby***

514 Root tips of young seedling were collected for Immuno-staining as previously described
515 (Zhao et al., 2019). *CRW* and *Bilby* were labeled with biotin-16-Dutp and
516 digoxigenin-11-dUTP via nick translation respectively. The hybridized probes were detected
517 by fluorescein-conjugated goat anti-biotin and anti-digoxigenin-rhodamine Fab fragments
518 coupled with TAMRA respectively. CENH3 was identified with anti-CENH3 antibody
519 detected by Goat anti-Rabbit IgG (H+L) conjugated Alexa Fluor 647. Images were taken by a
520 confocal (ZEISS LSM880) and processed using Adobe Photoshop CS.

521 **PPR gene analysis**

522 The genome sequence data and gene annotation of CS were downloaded from EnsemblPlants
523 (http://plants.ensembl.org/index.html). PPR sequences were annotated by Pfam databases
524 (http://pfam.xfam.org/, v.32.0), and IPR database (https://www.ebi.ac.uk/interpro/, v.77.0),
525 respectively. The classification of PPR was referred to Cheng et al. (Cheng et al., 2016). The
526 PPR gene collinearity between 1RS of AK58 and 1BS of CS was analyzed by best reciprocal
527 hit BLAST (*E-value* cutoff of 1e-5) (Gabriel and Kristen, 2007). The PPR gene's subcellular
528 localization was predicted using PSI (http://bis.zju.edu.cn/psi/) and validated by experiment.
529 In briefly, full-length PPR cDNA was amplified and inserted in front of a GFP-coding
530 sequence on the pUC-35S-EGFP vector. Tobacco (*Nicotiana benthamiana*) protoplasts were

531 prepared and transfected according to the method described by Shan et al (2014). The
532 protoplasts were subsequently stained with 10μm MitoTracker™ Orange CMTMRos
533 (Invitrogen, M7510) for 10 min, and then examined on using a confocal scanning microscope
534 system (ZEISS LSM880).

535 **The grain storage protein gene analysis**

536 Prolamin super-family genes identified in the wheat reference genome were used to manually
537 annotate the prolamin genes in the AK58 genome sequence (IWGSC et al., 2018; Juhász et al.,
538 2018). Translated sequences were checked for the presence of signal peptides and the
539 conserved cysteine pattern and Pfam domains as previously described (Juhász et al., 2018).
540 Obtained sequences were aligned with gliadins and secalins retrieved from the Uniprot
541 database to confirm the protein sub-types. Expression of genes was analyzed using the grain
542 specific transcriptome data set obtained from 4, 10, 15 and 20 DPA grain libraries. Protein
543 level expression of the translated secalins and nsLTPs were analyzed using the published data
544 (Bose et al., 2019). LC-MS-MS data originally generated from tryptic digests of rye flour
545 protein extracts were re-analyzed and protein identification was undertaken using
546 ProteinPilotTM 5.0 software (SCIEX) with the Paragon and ProGroup algorithms with
547 searches conducted against the Poaceae subset of the Uniprot database appended with the
548 identified 1RS gene models and a contaminant database (Common Repository of Adventitious
549 Proteins) (Shilov et al., 2007). Obtained fully tryptic peptides were mapped to the secalin and
550 nsLTP sequences in CLC Genomics Workbench v12 (Qiagen, Aarhus, Denmark) using 100%
551 sequence identity to confirm the expression at individual protein levels.

552 **RGA gene analysis**

553 To predict RGAs in AK58 genome, a new plant RGAs database was constructed using protein
554 sequences from the RGAdb (https://bitbucket.org/yaanlpc/rgaugury/src/master/) and candidate
555 RGAs predicted in *Ae. tauschii* genome (Li et al., 2016; Luo et al., 2017). A total of 61372
556 disease resistance related sequences were obtained. Protein sequences of all annotated genes
557 of AK58 were aligned to the new RGAs database using BLASTP with *E-value* cutoff of 1e-5.
558 Potential RGAs were selected based on rule 80:80:80 (query sequence coverage more than

559 80%, target sequence coverage more than 80 and identity more than 80%). Eight
560 RGAs-related domains and motifs including NB-ARC, NBS, LRR, TM, STTK, LysM, CC
561 and TIR were searched and identified by RGAugury pipeline (Li et al., 2016). RGA
562 candidates were predicted in *T. aestivum* (CS) genome using the same method.

563 **ACKNOWLEDGES**

564 The authors are grateful to Yaoguang Liu and his laboratory team from the College of Life
565 Sciences of the South China Agricultural University for suggestions in analyzing PPR gene
566 family. This research was supported by The National Key Research and Development
567 Program of China (2016YFD0101802 and 2016YFD0101602), Talent Program and
568 Innovation Program of CAAS.

569 **AUTHOR CONTRIBUTIONS**

570 ZR, DC, JJ, RA, and XK initiated the project and designed the study. AJ, DL, PD, ZJ, LF, KW,
571 GKG, ZY, GL, DW, UB, MC, CK, GZ, XZ, XL, GC, YW, ZN, and LW performed the
572 research. AJ, DL, PD, ZJ, LF, KW, GKG, CK, and GZ generated and analyzed the data. RA,
573 XK, JJ, AJ, DL, PD, ZJ and KW wrote the paper.

574 **CONFLICT OF INTEREST**

575 The authors have no conflicts of interest to declare.

576 **DATA AVAILABILITY**

577 The whole genome sequence data reported in this paper have been deposited in the Genome
578 Warehouse in National Genomics Data Center, Beijing Institute of Genomics (China National
579 Center for Bioinformation), Chinese Academy of Sciences, under accession number
580 GWHANRF00000000 that is publicly accessible at https://bigd.big.ac.cn/gwh. And the
581 Assembly and availability of 1RS.1BL genome sequence can be found in URGI,
582 https://urgi.versailles.inra.fr/download/iwgsc/AK58_1RS.1BL/.

583 **SUPPORTING INFORMATION**

584 **Figure S1.** Protein-coding gene prediction process overview.

585 **Figure S2.** Neighbor-joining phylogenetic tree for SNP analysis of 36 1RS.1BL lines.

586 **Figure S3.** Distribution of some of the dominant retrotransposable elements in 1RS.The
587 elements are identified on the right-hand side together with a color scale indicating the
588 relative prominence of the elements.

589 **Figure S4.** Transcript analysis.

590 **Table S1.** Pedigrees of wheat lines used for 660k SNP analysis.

591 **Table S2.** 1RS dominant TE information.

592 **Table S3.** PPR genes identified on the CS genome and their expression levels in different
593 tissues.

594 **Table S4.** PPR genes located on the region of Rf^{multi}.

595 **Table S5.** PPR Genes identified on the AK58 genome and their expression levels in different
596 tissues.

597 **Table S6.** Orthologous PPR genes from 1BS (CS) and 1RS (AK58).

598 **Table S7.** Orthologous genes from 1BS (CS) and 1RS (AK58) on the region of Rf^{multi}/rf^{multi}.

599 **Table S8.** PCR primers used in this study for subcellular localization.

600 **Table S9.** RGA Gene models analysis on the AK58 genome.

601 **Table S10.** A summary of the gene models in the morpheus clusters for contig-356, -445, -517
602 and -624 in the 1RS.1BL assembly.

603 **REFERENCES**

604 **Appels, R., Driscoll, C. and Peacock, W. J.** (1978). Heterochromatin and highly repeated
605 DNA sequences in rye (*Secale cereale*). *Chromosoma*, **70**, 67-89.

606 **Bartoš, P. and Bareš, I.** (1971). Leaf and stem rust resistance of hexaploid wheat cultivars
607 salzmünder bartweizen and weique. *Euphytica*, **20**, 435-440.

608 **Bauer, E., Schmutzer, T., Barilar, I., Mascher, M. and Scholz, U.** (2016). Towards a
609 whole-genome sequence for rye (*Secale cereale* L.). *Plant J.* **89**, 853.

610 **Bose, U., Broadbent, J.A., Byrne, K., Hasan, S., Howitt, C.A., and Colgrave, M.L.** (2019).
611 Optimisation of protein extraction for in-depth profiling of the cereal grain proteome. J.
612 *Proteomics*, **197**, 23-33.

613 **Cheng, H., Liu, J., Wen, J., Nie, X. and Jiang, Y.** (2019). Frequent intra- and inter-species
614 introgression shapes the landscape of genetic variation in bread wheat. *Genome Biol*. **20**,
615 136.
616 **Cheng, S., Gutmann, B., Zhong, X., Ye, Y., Fisher, M.F., Bai, F., Castleden, I., Song, Y.,**
617 **Song, B., Huang, J., et al.** (2016). Redefining the structural motifs that determine RNA
618 binding and RNA editing by pentatricopeptide repeat proteins in land plants. *Plant J*. **85**,
619 532-547.
620 **Clarke, B. C., Mukai, Y. and Appels, R.** (1996). The *Sec-1* locus on the short arm of
621 chromosome 1R of rye (*Secale cereale*). *Chromosoma*, **105**, 269-275.
622 **Crespo-Herrera, L. A., Garkava-Gustavsson, L. and Ahman, I.** (2017). A systematic
623 review of rye (*Secale cereale* L.) as a source of resistance to pathogens and pests in wheat
624 (*Triticum aestivum* L.). *Hereditas*, **154**, 14.
625 **Ehdaie, B., Whitkus, R. W. and Waines, J. G.** (2003). Root biomass, water-use efficiency,
626 and performance of wheat–rye translocations of chromosomes 1 and 2 in spring bread wheat
627 'Pavon'. *Crop Sci*. **43**, 710.
628 **Francki, M. G.** (2001). Identification of Bilby, a diverged centromeric Ty1-copia
629 retrotransposon family from cereal rye (*Secale cereale* L.). *Genome*, **44**, 266-274.
630 **Fu, S., Chen, L., Wang, Y., Li, M., Yang, Z., Qiu, L., Yan, B., Ren, Z., and Tang, Z.** (2015).
631 Oligonucleotide probes for ND-FISH analysis to identify rye and wheat chromosomes. *Sci.*
632 *Rep*. **5**, 10552.
633 **Gabriel, M. H. and Kristen, L.** (2007). Choosing BLAST options for better detection of
634 orthologs as reciprocal best hits. *Bioinformatics,* **24**, 319-324.
635 **Gobaa, S., Bancel, E., Kleijer, G., Stamp, P. and Branlard, G.** (2007). Effect of the
636 1BL.1RS translocation on the wheat endosperm, as revealed by proteomic analysis.
637 *Proteomics*, **7**, 4349-4357.
638 **Han, F., Lamb, J. C. and Birchler, J. A.** (2006). High frequency of centromere inactivation
639 resulting in stable dicentric chromosomes of maize. *Proc. Natl. Acad. Sci. USA*, **103**,
640 3238-3243.

641 **Henry, R. J., Martin, D. J. and Stewart, B. G.** (1989). Cell-wall polysaccharides of
642 rye-derived wheats, investigations of the biochemical causes of dough stickiness. *Food*
643 *Chem*. **34**, 309-316.
644 **Howell, T., Hale, I., Jankuloski, L., Bonafede, M., Gilbert, M., and Dubcovsky, J.** (2014).
645 Mapping a region within the 1RS.1BL translocation in common wheat affecting grain yield
646 and canopy water status. *Theor. Appl. Genet*. **127**, 2695-2709.
647 **Howell, T., Moriconi, J.I., Zhao, X., Hegarty, J., Fahima, T., Santa-Maria, G.E., and**
648 **Dubcovsky, J.** (2019). A wheat/rye polymorphism affects seminal root length and yield
649 across different irrigation regimes. *J. Exp. Bot*. **70**, 4027-4037.
650 **Hurni, S., Brunner, S., Buchmann, G., Herren, G., Jordan, T., Krukowski, P., Wicker, T.,**
651 **Yahiaoui, N., Mago, R., Keller, B.** (2013). Rye *Pm8* and wheat *Pm3* are orthologous genes
652 and show evolutionary conservation of resistance function against powdery mildew. *Plant J*.
653 **76**, 957-969.
654 **International Wheat Genome Sequencing Consortium(IWGSC), et al.** (2018). Shifting
655 the limits in wheat research and breeding using a fully annotated reference genome. *Science*,
656 **361,** eaar7191.
657 **Juhász, A., Belova, T., Florides, C.G., Maulis, C., Fischer, I., Gell, G., Birinyi, Z., Ong, J.,**
658 **Keeble-Gagnère, G., Maharajan, A., et al.** (2018). Genome mapping of seed-borne
659 allergens and immunoresponsive proteins in wheat. *Sci. Adv*. **4**, eaar8602.
660 **Keeble-Gagnère, G., Rigault, P., Tibbits, J., Pasam, R., Hayden, M., Forrest, K., Frenkel,**
661 **Z., Korol, A., Huang, B.E., Cavanagh, C., et al.** (2018). Optical and physical mapping
662 with local finishing enables megabase-scale resolution of agronomically important regions
663 in the wheat genome. *Genome Biol*. **19**, 112.
664 **Keeble-Gagnère, G., Isdale, D., Suchecki, R.-I., Kruger, A., Lomas, K., Carroll, D., Li, S.,**
665 **Whan, A., Hayden, M., and Tibbits, J.** (2019). Integrating past, present and future wheat
666 research with Pretzel. bioRxiv, 517953.
667 **Kelley, L. A., Mezulis, S., Yates, C. M., Wass, M. N. and Sternberg M. J.** (2015). The
668 Phyre2 web portal for protein modeling, prediction and analysis. *Nat. Protoc*. **10,** 845-858.

669 **Kucherov, G., Noé, L., Noé, L. and Roytberg, M.** (2006). A unifying framework for seed
670 sensitivity and its application to subset seeds. *J. Bioinform. Comput. Biol*. **4**, 553-569.
671 **Kumar, S., Stecher, G. and Tamura, K.** (2016). MEGA7, molecular evolutionary genetics
672 analysis version 7.0 for bigger datasets. *Mol. Biol. Evol*. **33**, 1870-1874.
673 **Langmead, B. and Salzberg, S. L.** (2012). Fast gapped-read alignment with Bowtie 2. *Nat.*
674 *Methods*, **9**, 357-359.
675 **Lang, T., Li, G., Wang, H., Yu, Z., Chen, Q., Yang, E., Fu, S., Tang, Z., and Yang, Z.**
676 (2019). Physical location of tandem repeats in the wheat genome and application for
677 chromosome identification. *Planta*, **249**, 663-675.
678 **Lawrence, G. J. and Appels, R.** (1986). Mapping the nucleolus organizer region, seed
679 protein loci and isozyme loci on chromosome 1R in rye. *Theor. Appl. Genet*. **71**, 742-749.
680 **Lee, J. H., Graybosch, R. A. and Peterson, C. J.** (1995). Quality and biochemical effects of
681 a 1BL/1RS wheat-rye translocation in wheat. *Theor. Appl. Genet*. **90**, 105-112.
682 **Lee, E., Helt, G. A., Reese, J. T., Munoz-Torres, M. C. and Lewis, S. E.** (2013). Web
683 Apollo, A web-based genomic annotation editing platform. *Genome Biol*. **14**, R93.
684 **Li, B., Choulet, F., Heng, Y., Hao, W., Paux, E., Liu, Z., Yue, W., Jin, W., Feuillet, C., and**
685 **Zhang, X.** (2013). Wheat centromeric retrotransposons, the new ones take a major role in
686 centromeric structure. *Plant J*. **73**, 952-965.
687 **Li, P., Quan, X., Jia, G., Xiao, J., Cloutier, S., and You, F.M.** (2016). RGAugury, a pipeline
688 for genome-wide prediction of resistance gene analogs (RGAs) in plants. *BMC Genomics*,
689 **17**, 852.
690 **Li, Z., Ren, T., Yan, B., Tan, F., Yang, M., and Ren, Z.** (2016). A mutant with expression
691 deletion of gene *Sec-1* in a 1RS.1BL line and its effect on production quality of wheat. *PLoS*
692 *ONE*, **11**, e0146943.
693 **Liu, C., Song, Q., Zhang, H., Yang, Z. and Hu, Y.** (2017). Molecular cytogenetic
694 characterization and phenotypic evaluation of new wheat–rye lines derived from hexaploid
695 triticale 'Certa'×common wheat hybrids. *Plant Breeding*, **136**, 809-819.
696 **Lukaszewski, A. J.** (2000). Manipulation of the 1RS.1BL translocation in wheat by induced
697 homoeologous recombination. *Crop Sci*. **40**, 216-225.

698 **Lukaszewski, A. J.** (2017). Chromosomes 1BS and 1RS for control of male fertility in
699 wheats and triticales with cytoplasms of *Aegilops kotschyi*, *Ae. mutica* and *Ae. uniaristata*.
700 *Theor. Appl. Genet*. **130**, 2521-2526.
701 **Lurin, C., Andrés, C., Aubourg, S., Bellaoui, M., Bitton, F., Bruyère, C., Caboche, M.,**
702 **Debast, C., Gualberto, J., Hoffmann, B., et al.** (2004). Genome-wide analysis of
703 Arabidopsis pentatricopeptide repeat proteins reveals their essential role in organelle
704 biogenesis. *Plant Cell*, **16**, 2089-2103.
705 **Luo, M.C., Gu, Y.Q., Puiu, D., Wang, H., Twardziok, S.O., Deal, K.R., Huo, N., Zhu, T.,**
706 **Wang, L., Wang, Y., et al.** (2017). Genome sequence of the progenitor of the wheat D
707 genome *Aegilops tauschii*. *Nature*, **551**, 498-502.
708 **Mago, R., Spielmeyer, W., Lawrence, J., Lagudah, S., Ellis, G., and Pryor, A.** (2002).
709 Identification and mapping of molecular markers linked to rust resistance genes located on
710 chromosome 1RS of rye using wheat-rye translocation lines. *Theor. Appl. Genet*. **104**,
711 1317-1324.
712 **Mago, R., Miah, H., Lawrence, G.J., Wellings, C.R., Spielmeyer, W., Bariana, H.S.,**
713 **McIntosh, R.A., Pryor, A.J., and Ellis, J.G.** (2005). High-resolution mapping and mutation
714 analysis separate the rust resistance genes *Sr31*, *Lr26* and *Yr9* on the short arm of rye
715 chromosome 1. *Theor. Appl. Genet*. **112**, 41-50.
716 **Mago, R., Zhang, P., Vautrin, S., Šimková, H. and Dodds, P. N.** (2015). The wheat *Sr50*
717 gene reveals rich diversity at a cereal disease resistance locus. *Nat. Plants*, **1**, 15186.
718 **Marçais, G., Delcher, A.L., Phillippy, A.M., Coston, R., Salzberg, S.L., and Zimin, A.**
719 (2018). MUMmer4, a fast and versatile genome alignment system. *PLoS Comput. Biol*. **14**,
720 e1005944.
721 **McIntyre, C. L., Pereira, S., Moran, L. B. and Appels, R.** (1990). New *Secale cereale* (rye)
722 DNA derivatives for the detection of rye chromosome segments in wheat. *Genome*, **33**,
723 635-640.
724 **Miedaner, T., Hübner, M., Korzun, V., Schmiedchen, B. and Reif, J. C.** (2012). Genetic
725 architecture of complex agronomic traits examined in two testcross populations of rye
726 (*Secale cereal* L.). *BMC Genomics*, **13**, 706.

Nagaki, K., Talbert, P.B., Zhong, C.X., Dawe, R.K., Henikoff, S., and Jiang, J. (2003). Chromatin immunoprecipitation reveals that the 180-bp satellite repeat is the key functional DNA element of *Arabidopsis thaliana* centromeres. *Genetics*, **163**, 1221-1225.

Rajaram S., Mann C. E., Ortiz-Ferrara G. and Mujeeb-Kazi A. (1983). Adaptation, stability and high yield potential of certain 1B/1R CIMMYT wheats. *In, S. Sakamoto (Ed). Proc. 6th Int. Wheat Genet. Symp., Kyoto, Japan*, 613-621.

Ramírez-González, R.H., Borrill, P., Lang, D., Harrington, S.A., Brinton, J., Venturini, L., Davey, M., Jacobs, J., van Ex, F., Pasha, A., et al. (2018). The transcriptional landscape of polyploid wheat. *Science*, **361**, eaar6089.

Schlegel, R. and Korzun, V. (1997). About the origin of 1RS.1BL wheat-rye chromosome translocations from Germany. *Plant Breeding*, **116**, 537-540.

Shan, Q., Wang, Y., Li, J., and Gao, C. (2014). Genome editing in rice and wheat using the CRISPR/Cas system. *Nat. Protoc*. **9**, 2395-2410.

Sharma, S., Bhat, P.R., Ehdaie, B., Close, T.J., Lukaszewski, A.J., and Waines, J.G. (2009). Integrated genetic map and genetic analysis of a region associated with root traits on the short arm of rye chromosome 1 in bread wheat. *Theor. Appl. Genet*. **119**, 783-793.

Sharma, S., Xu, S., Ehdaie, B., Hoops, A., Close, T.J., Lukaszewski, A.J., and Waines, J.G. (2011). Dissection of QTL effects for root traits using a chromosome arm-specific mapping population in bread wheat. *Theor. Appl. Genet*. **122**, 759-769.

Shilov, I.V., Seymour, S.L., Patel, A.A., Loboda, A., Tang, W.H., Keating, S.P., Hunter, C.L., Nuwaysir, L.M., and Schaeffer, D.A. (2007). The Paragon Algorithm, a next generation search engine that uses sequence temperature values and feature probabilities to identify peptides from tandem mass spectra. Mol. Cell. *Proteomics*, **6**, 1638-1655.

Sukumaran, S., Dreisigacker, S., Lopes, M., Chavez, P. and Reynolds, M. P. (2015). Genome-wide association study for grain yield and related traits in an elite spring wheat population grown in temperate irrigated environments. *Theor. Appl. Genet*. **128**, 53-363.

Tang, Z., Yang, Z. and Fu, S. (2014). Oligonucleotides replacing the roles of repetitive sequences pAs1, pSc119.2, pTa-535, pTa71, CCS1, and pAWRC.1 for FISH analysis. *J. Appl. Genet.* **55**, 313-318.

Tsunewaki, K. (2015). Fine mapping of the first multi-fertility-restoring gene, *Rf*^{multi}, of wheat for three *Aegilops* plasmons, using 1BS-1RS recombinant lines. *Theor. Appl. Genet.* **128**, 723-732.

Waines, J. G. and Ehdaie, B. (2007). Domestication and crop physiology, roots of green-revolution wheat. *Ann. Bot*. **100**, 991-998.

Yan, R., Liang, C., Meng, Z., Malik, W., Zhu, T., Zong, X., Guo, S., and Zhang, R. (2016). Progress in genome sequencing will accelerate molecular breeding in cotton (*Gossypium spp.*). *3 Biotech*, **6**, 217.

Zhang, P., Li, W., Fellers, J., Friebe, B. and Gill, B. S. (2004). BAC-FISH in wheat identifies chromosome landmarks consisting of different types of transposable elements. *Chromosoma*, **112**, 288-299.

Zhao, J., Hao, W., Tang, C., Yao, H., Li, B., Zheng, Q., Li, Z., and Zhang, X. (2019). Plasticity in Triticeae centromere DNA sequences, a wheat × tall wheatgrass (decaploid) model. *Plant J*. **100**, 314-327.

Zeller, F. J. (1973). 1B/1R wheat-rye chromosome substitutions and translocations. *Proc. 4th Int. Wheat Genet. Symp., Missouri Agric. Exper. Station, Columbia, MO*, 209-221.

Table 1. RGAs prediction in AK58 1RS compared to CS 1AS, 1BS and 1DS, respectively.

Species	Chr	Have NB-ARC or TIR domain C: CC; N: NBS; L: LRR; T: TIR;				Has a TM domain STTK; TM; LRR; LysM; CC			Total
		CN	CNL	NBS	NL	RLK	RLP	TM-CC	
AK58	Chr1RS	8	39	4	13	74	4	7	149
	Chr1AS	6	20	1	8	39	2	1	77
CS	Chr1BS	10	30	14	18	41	4	1	118
	Chr1DS	5	28	4	10	37	5	2	91

775 **FIGURE LEGENDS**

776 **Figure 1.** Structure of the AK58 1RS.1BL chromosome.

777 (a) The high confidence (HC) gene models from the IWGSC-Refseq v1.0/-Refseq v2.0
778 assembly for chromosome 1B of CS wheat have been aligned with their syntenic partner gene
779 models in AK58 1RS.1BL using open source Pretzel (IWGSC et al., 2018; Keeble-Gagnère et
780 al., 2019).
781 (b) Summary of available genetic and cytogenetic details for the terminal 22 Mb region of
782 1RS showing 1RS (red)-1BS (yellow) recombinants that disrupt the yield attributes associated
783 with the 1RS.1BL chromosome (Howell et al., 2014 and 2019).
784 (c) *In situ* hybridization of repetitive sequence probes typically used to identify rye
785 chromosomes to allow a broad level validation of the 1RS assembly.
786 (d) Distribution of SNPs along representative sections of the 1RS.1BL chromosomes based on
787 a 660K SNP-chip analysis (Figure S2 and Table S1). Nine wheat cultivars (left most clusters)
788 and 36 1RS containing cultivars (remaining columns in the Figure) where the dark horizontal
789 lines indicate a SNP in the respective position that is different in AK58 reference genome
790 (blue box). Absence of a dark line indicates the alternate allele is the same as that in AK58.

791 **Figure 2.** The 1RS.1BL centromere.

792 (a) Dot-plot analysis of genome sequence at 245 Mb-315 Mb and BLAST-based distribution
793 of ChIP-Seq data based on the CENH3-precipitation in AK58 and CS. (a1) Dot matrix of the
794 AK58 centromere region of 70 Mb using YASS with the dashed-line boxes indicating the very
795 large blocks of repetitive sequences (Kucherov et al., 2006). (a2) Blast of CENH3-antibody
796 ChIP-Seq reads from CS on the 1RS.1BL centromere region showed two sub-domains which
797 basically consist of the *CRW* and *Quinta* TEs. (a3) Blast of CENH3-antibody ChIP-Seq reads
798 from AK58, the blast domain appears on the 1RS side (red) instead of 1BL relative to the
799 wheat CRW (green) and Quinta (blue). (a4) Distribution of retrotransposons in the 1RS.1BL
800 centromere region of AK58 - the boxes in dashed lines and solid lines are discussed in the text.
801 (a5) Dot matrix of the 70 Mb AK58 centromere region vs the 20 Mb core centromere region
802 from CS. The solid blue line boxes define regions addressed in the text.

803 (b) Late prophase nuclei (same in each frame) show the *in situ* co-localization of the CENH3
804 antibody (white), the rye Bilby sequence (red) and the Cereba (CRW, green) sequences. The
805 Bilby sequence (red) detects 1RS centromeres from the other 40 wheat centromeres (green).
806 The green dots conjugating with the red dot is the 1BL centromere. The CENH3 signals were
807 mainly co-located with the Bilby signals and this directly supports the centromere shift in
808 observed in Figure 2 (a3) in the BLAST analysis of AK58-CENH3 ChIP-Seq reads.

809 **Figure 3.** Comparative analysis of gene expression in group 1 chromosomes between AK58
810 and CS.

811 (a) Expression pattern of genes in 1RS (blue) and 1BS (yellow) shown as % of total gene
812 number expressed in the spike, root, grain and leaf tissues. Tissue-specific genes are
813 highlighted in darker shades both for 1RS (blue) and 1BS (yellow).
814 (b) Comparison of tissue-specificity in AK58 and CS with the numbers showing information
815 for each line and tissue as AK58/CS.
816 (c) Comparison of tissue specific gene expression across the short and long arms of the group
817 1 chromosomes. The 1BS/1RS panel highlights a major difference between AK58 and CS in
818 the grain-DPA20 stage where a 6.44-fold higher expression of transcripts in AK58 vs CS at
819 20DPA was identified.

820 **Figure 4.** PPR gene comparisons between 1RS of AK58 and 1BS of CS.

821 (a) Gene collinearity analysis.
822 (b) PPR gene expression comparison for the genes indicated in either orange (CS origin) or
823 AK58 (blue origin) for the tissues, seedling leaf, seedling root, FM (flowering meristem) and
824 grain tissue (DPA = days post anthesis).
825 (c) Subcellular localization of *TraesCS1B01G072300* and *TraesCS1B01G072900*. Protoplasts
826 transformed with 35S: GFP (pUC-35S-GFP), 35S:TraesCS1B01G072300-GFP
827 (*TraesCS1B01G072300*) and 35S:TraesCS1B01G072900-GFP (*TraesCS1B01G072900*)
828 constructs were analyzed using fluorescence microscopy. DIC indicated bright field. The dye
829 Mito-Tracker Orange was used as a mitochondrial marker. (Scale bars: 20 μm.).

830 **Figure 5.** The grain storage protein gene analysis.

831 (a) Gamma secalin locus on chromosome arm 1RS.

832 (b) Omega secalin locus on chromosome arm 1RS.

833 (c) nsLTP locus on chromosome arm 1RS.The tracks underneath each of genome map
834 locations provide the level of expression at the respective stages of grain development and
835 evidence for the representation of the gene models as grain proteins in extensive rye proteome
836 studies.

837 **Figure 6.** Co-expression analysis of homologous genes expressed in the 22 Mb region of
838 AK58 1RS. Co-expression similarity values are represented in AK58 1RS calculated using
839 Pearson correlation followed by hierarchical clustering using the pre-computed similarity
840 matrix values. Co-expression values below -0.7 are labelled in blue and represent strong
841 negative co-expression. Co-expression above 0.7 represents strong expression similarity and
842 is highlighted in red. Tissue specificity and location of the genes within the analyzed contigs
843 in the 22 Mb region are highlighted with different colors. Matrix was generated using
844 https://software.broadinstitute.org/morpheus/.

845 **Figure 1**

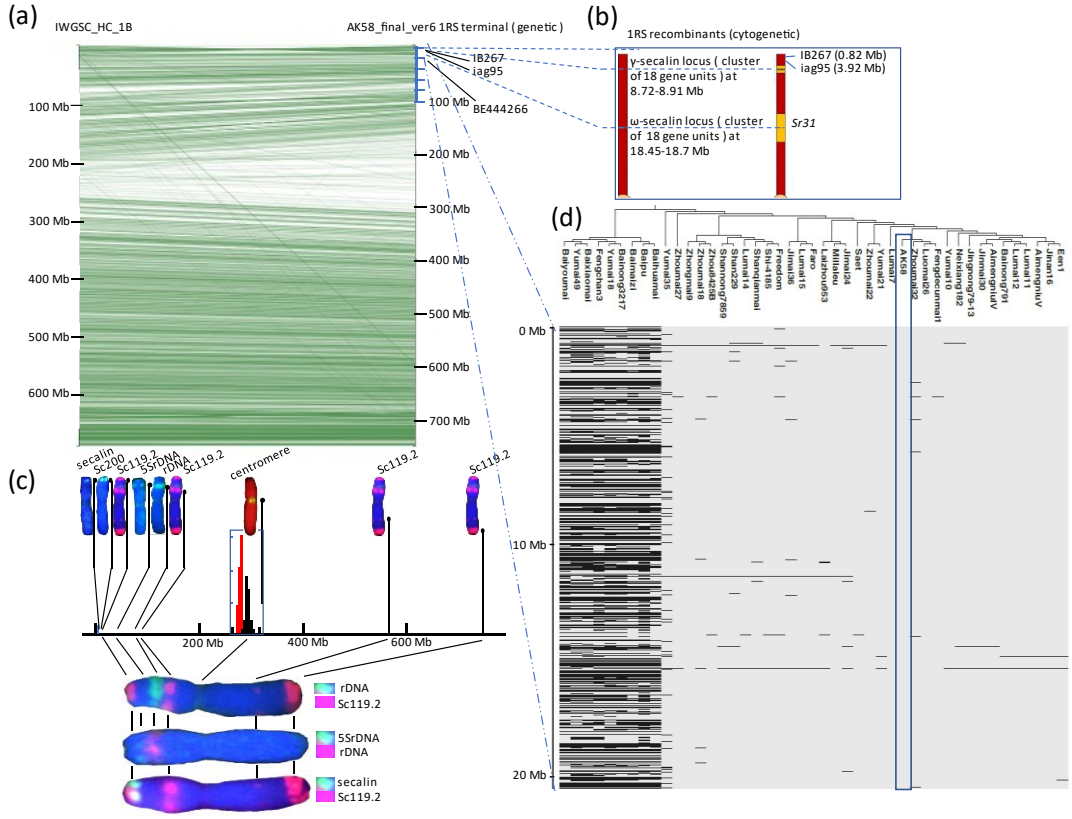

double labeling by *in situ* hybridization validates the relative positions of repetitive sequences

846 **Figure 2**

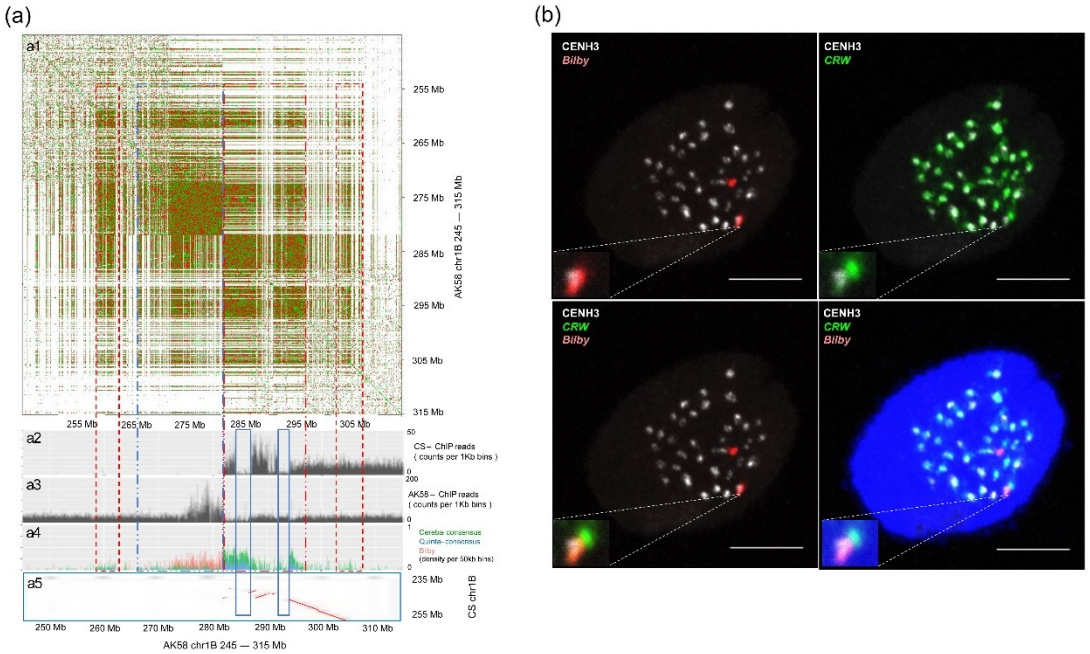

847 **Figure 3**

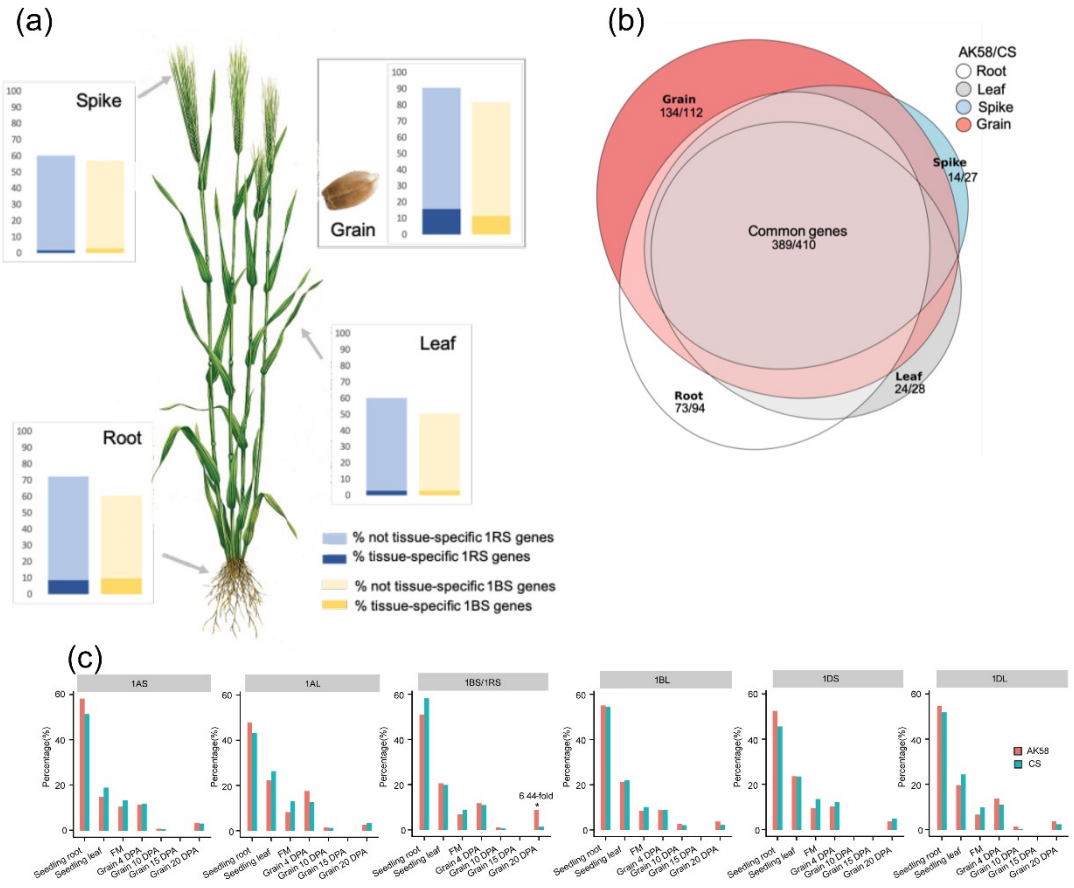
(a)
Spike
Grain
Leaf
Root
% not tissue-specific 1RS genes
% tissue-specific 1RS genes
% not tissue-specific 1BS genes
% tissue-specific 1BS genes
(b)
AK58/CS
Root
Leaf
Spike
Grain
Grain
134/112
Spike
14/27
Common genes
389/410
Leaf
24/28
Root
73/94
(c)
1AS
1AL
1BS/1RS
1BL
1DS
1DL
Percentage(%)
6.44-fold
AK58
CS
Seedling root
Seedling leaf
FM
Grain 4 DPA
Grain 10 DPA
Grain 15 DPA
Grain 20 DPA

848 **Figure 4**

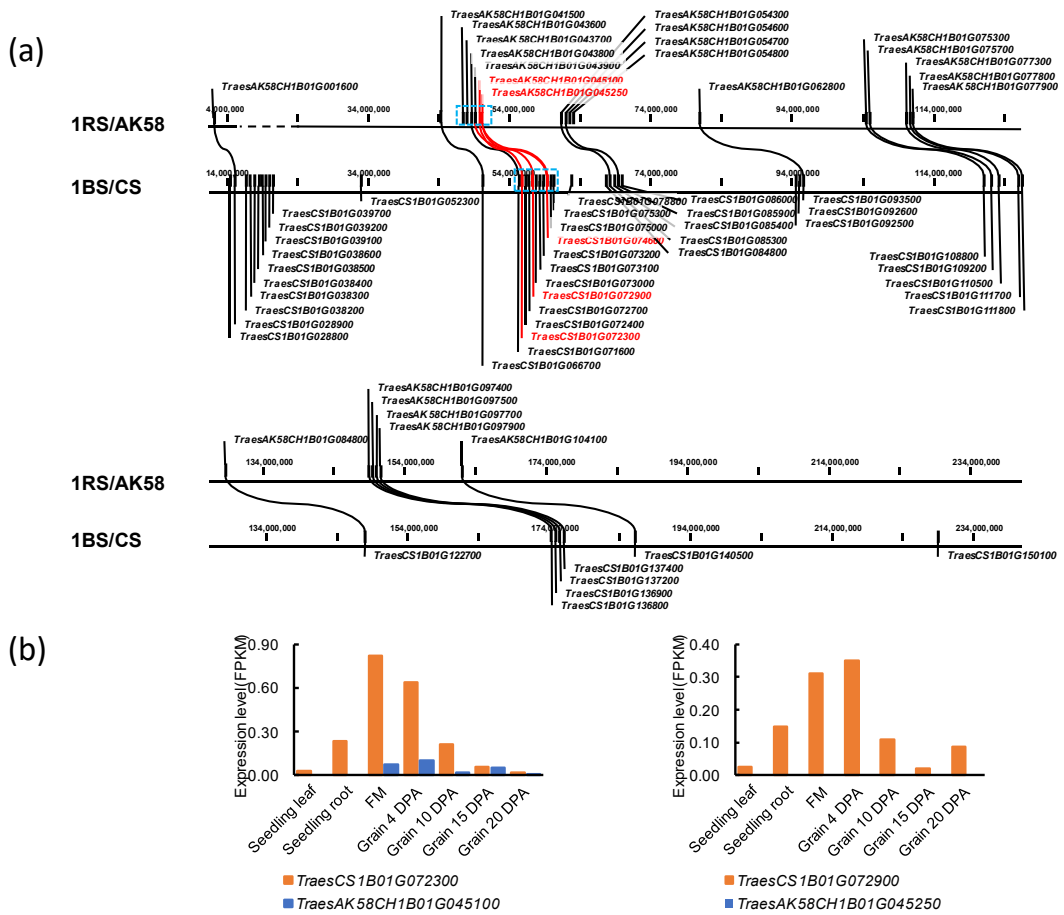
(a)
1RS/AK58
1BS/CS
TraesAK58CH1B01G001600
TraesAK58CH1B01G041500
TraesAK58CH1B01G043600
TraesAK58CH1B01G043700
TraesAK58CH1B01G043800
TraesAK58CH1B01G045100
TraesAK58CH1B01G045250
TraesAK58CH1B01G054300
TraesAK58CH1B01G054600
TraesAK58CH1B01G054700
TraesAK58CH1B01G054800
TraesAK58CH1B01G062800
TraesAK58CH1B01G075300
TraesAK58CH1B01G075700
TraesAK58CH1B01G077300
TraesAK58CH1B01G077800
TraesAK58CH1B01G077900
TraesCS1B01G052300
TraesCS1B01G039700
TraesCS1B01G039200
TraesCS1B01G039100
TraesCS1B01G038600
TraesCS1B01G038500
TraesCS1B01G038400
TraesCS1B01G038300
TraesCS1B01G038200
TraesCS1B01G028900
TraesCS1B01G028800
TraesCS1B01G075300
TraesCS1B01G075000
TraesCS1B01G073200
TraesCS1B01G073100
TraesCS1B01G073000
TraesCS1B01G072900
TraesCS1B01G072700
TraesCS1B01G072400
TraesCS1B01G072300
TraesCS1B01G071600
TraesCS1B01G066700
TraesCS1B01G086000
TraesCS1B01G085900
TraesCS1B01G085400
TraesCS1B01G085300
TraesCS1B01G084800
TraesCS1B01G093500
TraesCS1B01G092600
TraesCS1B01G092500
TraesCS1B01G108800
TraesCS1B01G109200
TraesCS1B01G110500
TraesCS1B01G111700
TraesCS1B01G111800
TraesAK58CH1B01G097400
TraesAK58CH1B01G097500
TraesAK58CH1B01G097700
TraesAK58CH1B01G097900
TraesAK58CH1B01G084800
TraesAK58CH1B01G104100
TraesCS1B01G122700
TraesCS1B01G137400
TraesCS1B01G137200
TraesCS1B01G136900
TraesCS1B01G136800
TraesCS1B01G140500
TraesCS1B01G150100
(b)
Expression level(FPKM)
Seedling leaf
Seedling root
FM
Grain 4 DPA
Grain 10 DPA
Grain 15 DPA
Grain 20 DPA
TraesCS1B01G072300
TraesAK58CH1B01G045100
TraesCS1B01G072900
TraesAK58CH1B01G045250
(c)
DIC
Mito-Tracker Orange
GFP
Merged
pUC-35S-EGFP
TraesCS1B01G072300
TraesCS1B01G072900
20 μm

849 **Figure 5**

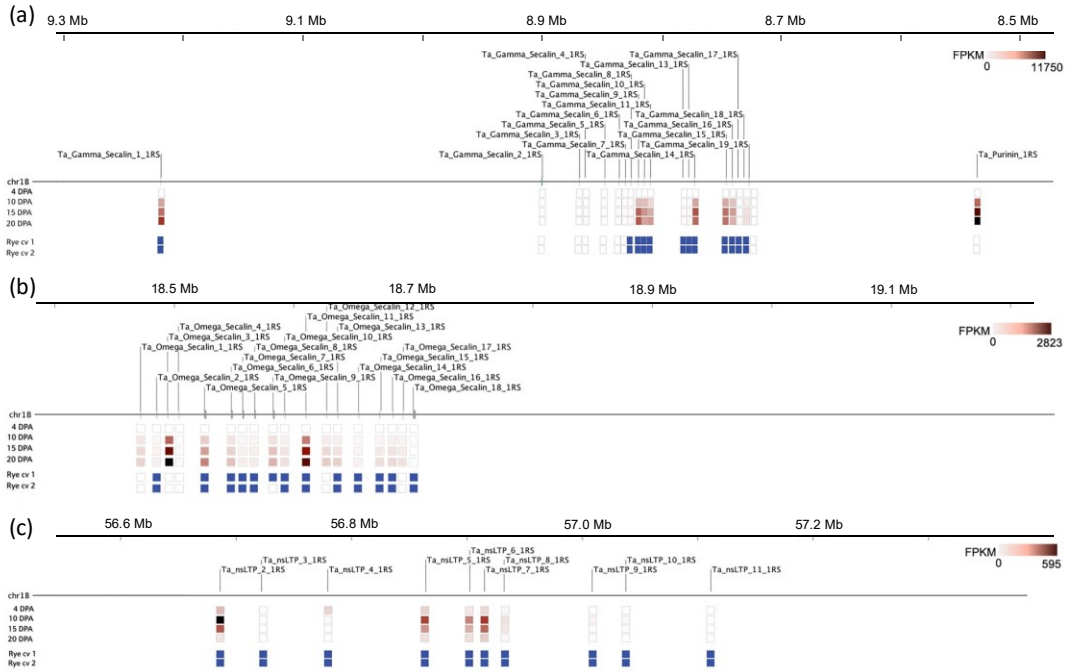
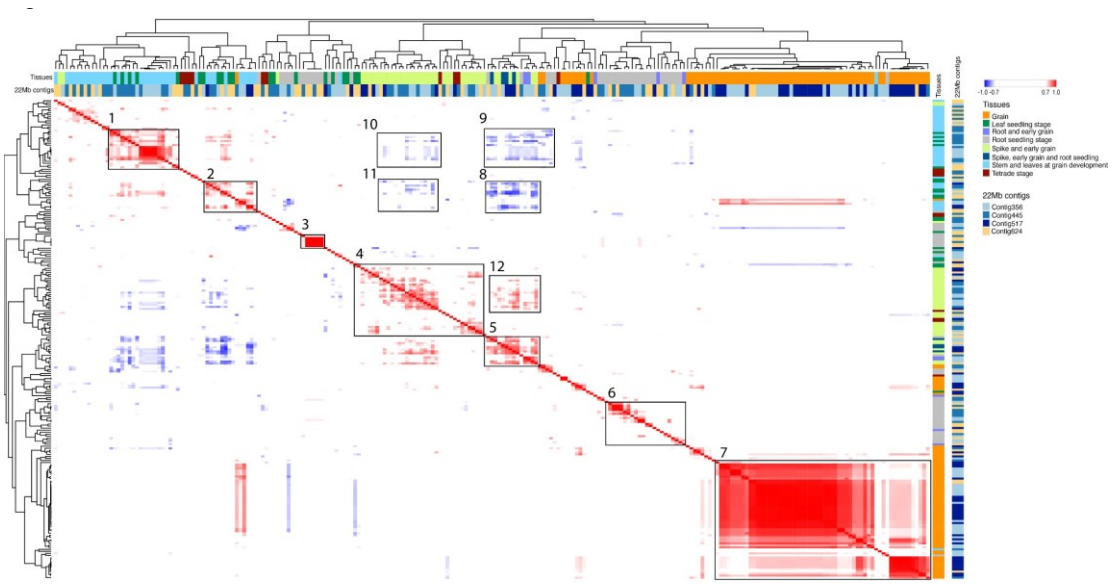
850 **Figure 6**